Eur. Phys. J. A (2023) 59:295
https://doi.org/10.1140/epja/s10050-023-01202-5

THE EUROPEAN PHYSICAL JOURNAL A

Regular Article - Experimental Physics

Global comparison between experimentally measured isomeric yield ratios and nuclear model calculations

Simone Cannarozzo[1,a], **Stephan Pomp**[1,b], **Andreas Solders**[1], **Ali Al-Adili**[1], **Alf Göök**[1], **Arjan Koning**[2]

[1] Department of Physics and Astronomy, Uppsala University, Box 516, Uppsala 751 20, Sweden
[2] Nuclear Data Section, IAEA, Wagrammerstrasse 5, Wien 1400, Austria

Received: 28 June 2023 / Accepted: 27 November 2023

Communicated by Wolfram Korten

Abstract The level density steers transition probabilities between different states in the decay and de-excitation of excited nuclei. Reliable level density modelling is, therefore, key in describing, e.g., de-excitation of fission fragments, with implications on neutron and gamma-rays multiplicities, and also manifested in the population of isomeric states. We test six currently used level density models and the spin distribution in the level density by comparing calculations with measured isomeric yield ratios. The model calculations are performed with the TALYS code and experimental data for nuclear reactions populating spin isomers are retrieved from the EXFOR database. On average, calculations are in agreement with measured data. However, we find that the population of the high-spin state in an isomeric pair is clearly favoured in all of the six studied level density models. Further studies are then performed on the three used phenomenological level density models, to investigate the significance of their effect. We find that a significant reduction of the spin width distribution improves the agreement between calculated and experimentally observed isomeric yield ratios. This result is independent of the incident particle in the nuclear reaction. The needed reduction of the spin width distribution to comply with empirical data has, e.g., implications for studies in angular momentum generation in fission using isomeric yield rations, calculations of anti-neutrino spectra from nuclear reactors, as well as neutron and gamma-ray multiplicities in nuclear reactor calculations.

1 Introduction

It is well known that fission fragments (FF) carry angular momenta far in excess of the angular momentum of the fissioning system [1]. The mechanism generating these angular momenta in the fission process is among the open challenges in fission research and has recently generated stimulating debates [2–7]. Since FF angular momenta are not directly observable, nuclear model calculations are invoked to derive empirical data from experimentally accessible observables that can be tested versus nuclear fission models.

A good description of nuclear level densities (LD), including a model for the spin distribution in the LD, is the most important ingredient of nuclear models for calculations of the de-excitation of the highly excited FF. Level density models (LDM) allow for calculating transition probabilities between different states in the de-excitation of FF, providing predictions of experimentally accessible observables.

Yield ratios for spin isomers produced in a fission reaction are one example of such an observable. Experimentally obtained data can be compared to predictions from proposed theoretical models for angular momentum generation in fission [8–12]. However, such comparisons depend on both the fission model and the LDM.

In this work, we test the capabilities of the six LDM implemented in nuclear model code TALYS v1.96 [13,14]. We compare results from model calculations with available experimental data for spin isomers. Experimental data on isomeric yield ratios (IYR), i.e. the ratio between the production yield of the ground and long-lived excited states of a nucleus, can be retrieved from the EXFOR database [15]. The amount of experimental data on isomeric yield ratios contained in EXFOR is extensive both regarding nuclear reactions [16] and fissions [17], and efforts are being made to correct possible inaccuracies [16].

Therefore, these data provide a good global testing ground for the models describing spin distributions in the level densities and can reveal effects that remain hidden when studying only a few selected cases. We choose to analyse data of nuclear reactions induced by photons and light particles

[a] e-mail: simone.cannarozzo@physics.uu.se (corresponding author)
[b] e-mail: stephan.pomp@physics.uu.se (corresponding author)

Published online: 14 December 2023

excluding fission because the angular momentum generation in fission is not yet well understood and initial conditions of the de-excitation process are influenced by additional factors, e.g., fission yields. Observed differences between calculated and experimental IYR might be attributed to both the models implemented in TALYS to calculate the entrance channel, e.g. the optical model, leading to a description of the population of excited states, and those describing the de-excitation process of this excited systems. The optical models and photon strength functions used in TALYS have been extensively tested and validated with a range of experimental data [14]. We therefore focus on studying the impact of the LD and the associated spin distribution which have a direct impact on the population of spin isomers. Recent studies have also shown that variations of the spin distributions of the level densities for the de-exciting nuclei may be needed to improve the agreement of experimental and calculated data. Specifically, studies with different nuclear model codes like TALYS and FIFRELIN [16,18–20] show that the width of the spin distribution of the level densities may be overestimated, and thus a correction factor needs to be added. For these reasons, in this work we decided to study the effect of LDMs and specifically the width of their spin distributions. We investigate this possible correction needed by making use of a large dataset and investigating the link to the spin of the isomeric states of the produced nucleus.

2 Method

The database of experimentally measured IYRs used in this work is built by retrieving data from the Experimental Nuclear Reaction Data (EXFOR) library (Sect. 3), where they are organized in entries. They are the basic unit of the library and each one corresponds to one specific experiment described in one or more bibliographic references [15]; i.e. one entry consists of one or more measured IYRs. TALYS calculations are performed for all the data points in the selected EXFOR entries (Sect. 4) and then compared with the experimental information. Thereafter, figures of merit representative of the code's accuracy are calculated for every EXFOR entry and then collected to study the general performances (Sect. 5). This process is performed both on the complete dataset and on sub-sets, where data are collected on the basis of common features: incident projectiles of the reaction, and whether the ground state or the excited state is the high-spin state. It is also repeated for both different LDM implemented in TALYS, and for different values of the parameter influencing the width of the spin distribution of the level densities. The results then allow for studying the influence of the parameters on the agreement of the calculations with the experimental evidence (Sect. 6).

Table 1 Composition of the database divided into the six possible projectile particles, showing both the number of entries and experimental data

Projectile	Entries	Experimental data
n	498	1382
γ	290	1245
α	151	1243
p	138	999
d	40	334
h	13	156
Total	1130	5359

3 Experimental data

For this study, it was possible to retrieve from the EXFOR library (version of the 2023-02-13) 1.131 entries involving 182 nuclei, for a total of 5.404 experimentally measured IYRs, divided by incident particle as shown in Table 1 and distributed by proton and neutron number as illustrated in Fig. 1. Each entry reports the numerical data of one specific reaction and can contain more than one datapoint (IYR) in case the IYRs were measured at different projectile energies. The entries used in this work were chosen following the constraints on what TALYS can reproduce, that is reactions involving light incident particles (neutrons, protons, deuterons, ^3He, and α particles) and photons with an energy lower than 200 MeV. Thus the EXFOR queries are based on the following request fields: parameters (*SIG/RAT*, respectively cross section and ratio), projectile (n, p, d, h, a) and energy. Two more practical constraints were imposed on the entries in order to use them. The first one is that the target nucleus was one single isotope, not an element in its natural isotopic composition. The second constrain is related to the definition of IYR. In the context of this work, it is defined as:

$$\mathrm{IYR} = \frac{Y_e}{Y_e + Y_g} \tag{1}$$

where Y_e and Y_g are the yields of the excited and the ground state, respectively. In the EXFOR database, several different definitions of the IYR are used. As long as the ratio is defined based on the energy of the status the entries can be easily converted to the format of Eq 1. However, for a small number of entries (7 in total) the IYR is defined based on the yields of high and low-spin states. These entries are not as straightforward to convert and were therefore omitted in the study.

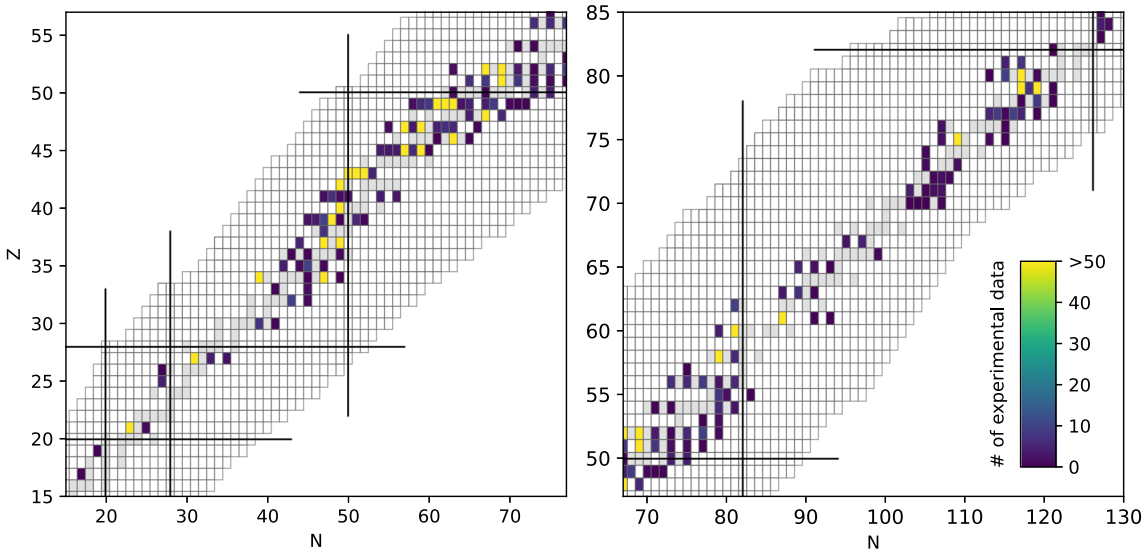

Fig. 1 Distribution of the nuclei included in the IYR database used in this work on the nuclear chart

4 Nuclear model code and calculations

Several TALYS calculations are run for each experimental IYR, where models and parameters of the calculation are changed. Thus we can compare the different LDM and the variation of the width of the spin distributions. We do so by repeating the simulations of the 5359 experimental datapoints at different values and comparing the results through the analysis process described in Sect. 5.

Six LDMs are implemented in TALYS, three of them use a phenomenological approach, being Constant Temperature + Fermi gas model (CTM) [21], Back-shifted Fermi gas Model (BFM) [22], Generalised Superfluid Model (GSM) [23], and three use tabulated level densities derived from microscopic models [14,24–26]. These models are used by TALYS to compute the level density $\rho(E_x, J, \Pi)$ which is defined as the number of nuclear levels around an excitation energy E_x for a certain spin J and parity Π [27]. In the case of phenomenological models, it is usually factorized as follows:

$$\rho(E_x, J, \Pi) = P(E_x, J, \Pi) R(E_x, J) \rho_{tot}(E_x) \tag{2}$$

where $P(E_x, J, \Pi)$ is the parity distribution, $\rho_{tot}(E_x)$ is the total LD and $R(E_x, J)$ is the spin distribution [27]. The LD can be calculated in several ways depending on the model and the energy of the nucleus. In the Fermi gas model [14], which is used in CTM and BFM, it has the following form:

$$\rho_F(E_x, J, \Pi) = \frac{1}{2} \frac{2J+1}{2\sqrt{2\pi}\sigma^2} \exp\left[-\frac{\left(J+\frac{1}{2}\right)^2}{2\sigma^2}\right] \frac{\sqrt{\pi}}{12} \frac{\exp\left[2\sqrt{aU}\right]}{a^{1/4}U^{5/4}} \tag{3}$$

In this equation U is the effective excitation energy and a is an energy-dependent parameter called the level density parameter. Equation 3 also contains the so-called spin cut-off parameter σ^2. It defines the width of the spin distribution of the LD and it is represented by different equations, depending on the model and the energy of the nucleus. For example, in CTM and for energies larger than the neutron separation energy [14], it is derived from the undeformed moment of inertia I_0 and the thermodynamic temperature t as follows:

$$\sigma_F^2(E_x) = I_0 \frac{a}{\tilde{a}} t = 0.01389 \frac{A^{5/3}}{\tilde{a}} \sqrt{a(E_x)U} \tag{4}$$

Here $\tilde{a} = a(E_x \to \infty)$ is the asymptotic value of the level density parameter.

Regardless of the way it is calculated, the spin cut-off parameter σ^2 can be altered when using the phenomenological models in a TALYS calculation using a multiplication factor, in this work called R_{sc}, which scales the width of the spin distribution of the LD. It is not possible to apply this multiplication factor for the microscopic LDMs in the current release of TALYS, although this feature is expected to be present in future releases of the code. Hence we perform only default calculations for the microscopic LDM and study the impact of R_{sc} only for the phenomenological LDMs.

The standard value of R_{sc} is 1.0 and in this work, the effect of a variation between 0.25 and 1.5 is studied. The effect of such variation on the LD is displayed, as an example, in Fig. 2 for ^{94}Tc. This plot shows how the value of R_{sc} affects the width of the LD distributions.

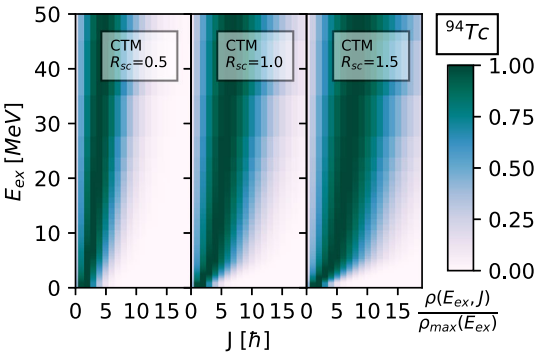

Fig. 2 Normalized nuclear level density distributions as a function of excitation energy and spin for ^{94}Tc, calculated with TALYS using CTM level density model.From left to right panel, the plots show how an increasing R_{sc} results in a larger width of the spin distributions

5 Analysis

The analysis process starts by calculating, for the i-th EXFOR entry, the weighted mean $\overline{X}_i$ of the differences between measured and calculated IYRs for each item in the entry. It is used as the estimator of the difference between experimental and calculated IYRs and it is defined as:

$$\overline{X}_i = \frac{\sum_{k=1}^{n} w_{i,k} x_{i,k}}{\sum_{k=1}^{n} w_{i,k}} \tag{5}$$

where k represents the single data points in the entry, n is the number of data points, $x_{i,k} = \mathrm{IYR}_{\mathrm{exp,i,k}} - \mathrm{IYR}_{\mathrm{TALYS,i,k}}$, and $w_{i,k}$ is the squared inverse of the uncertainty of the experimental IYR as given in EXFOR. The value of $\overline{X}_i$ is calculated for each entry. This first step is performed in order to condense the information regarding one experiment in one figure of merit ($\overline{X}_i$), avoiding a small number of isotopes from being over-represented, as showed in Fig. 1. As an example, the database contains 236 experimental data-points where ^{58}Co is produced, for a total of 36 entries, i.e. individual measurement campaigns.

No uncertainty is assigned to $\overline{X}_i$ due of the significant compilation and evaluation challenge of comparing the uncertainties of a large variety of experiments, measurement techniques, error analysis methods and error definitions.

After the first step, all the $\overline{X}_i$ are collected in a frequency distribution, and the mean value $\langle \overline{X} \rangle$ and its standard error SE for the data-set are calculated as:

$$\begin{aligned} \langle \overline{X} \rangle &= \frac{\sum_{i=1}^{m} \overline{X}_i}{m} \\ SE &= \sqrt{\frac{\sum_{i=1}^{m} (\overline{X}_i - \langle \overline{X} \rangle)^2}{m(m-1)}} \end{aligned} \tag{6}$$

where m is the total number of entries and $\overline{X}_i$ are the single weighted means, as defined in Eq. 5. Figure 3 shows the

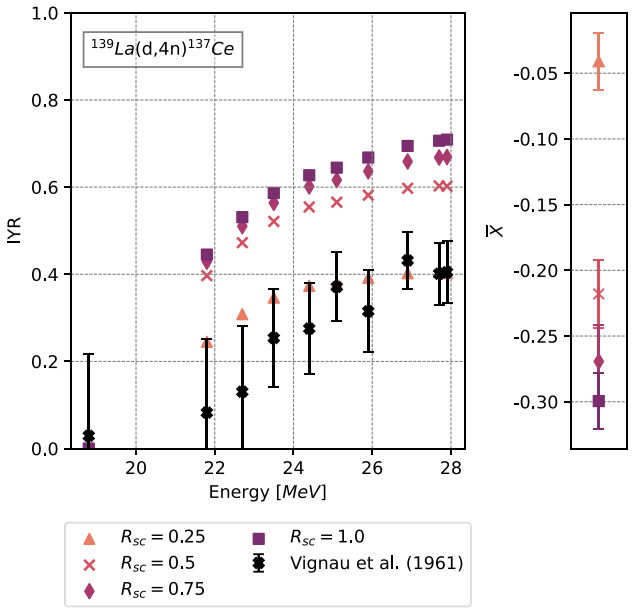

Fig. 3 On the left, experimental and calculated IYRs for the $^{139}La(d,4n)^{137}Ce$ reaction [28]. The calculation results are showed for different R_{sc} values. On the right, the corresponding $\overline{X}$. The spin of the ground and excited states of ^{137}Ce are $J_g = 3/2$ and $J_e = 11/2$, respectively

Table 2 Values of $\langle \overline{X} \rangle$, $\langle \overline{X} \rangle_{J_g > J_e}$ and $\langle \overline{X} \rangle_{J_g < J_e}$ for all the six LDM using default settings of TALYS ($R_{(sc)} = 1.0$). The three microscopic LDM are the Skyrme–Hartree–Fock–Bogoluybov (SHFB), Gogny–Hartree–Fock–Bogoluybov (GHFB), Temperature dependent Gogny–Hartree–Fock–Bogoluybov(TD-GHFB) models [14]

LDM	$\langle \overline{X} \rangle$	$\langle \overline{X} \rangle_{J_g > J_e}$	$\langle \overline{X} \rangle_{J_g < J_e}$
CTM	−0.006 (7)	0.04 (1)	−0.027 (7)
BFM	−0.009 (6)	0.04 (1)	−0.032 (7)
GSM	−0.006 (1)	0.05 (1)	−0.029 (7)
SHFB	−0.016 (7)	0.06 (1)	−0.047 (7)
GHFB	−0.025 (7)	0.06 (1)	−0.055 (7)
TD-GHFB	−0.015 (7)	0.07 (1)	−0.051 (6)

comparison between experimental and calculated IYRs for one specific experiment [28] and how the TALYS results change as a function of R_{sc}. In this example, it is evident that, while the trend of calculated data matches the experimental one, there is an overestimation of the high-spin state, which is reduced by decreasing R_{sc}. This is, however, one example and the illustrated behaviour is not representative of all entries.

The top plot of Fig. 4 shows the frequency density and weighted mean for the calculations performed with the default settings of TALYS (CTM and $R_{sc} = 1.0$). In this specific case, experimental data and TALYS calculations are on average in agreement, as the most probable value of $\overline{X}$ corresponds to the bin centered around zero and $\langle \overline{X} \rangle = -0.01(1)$.

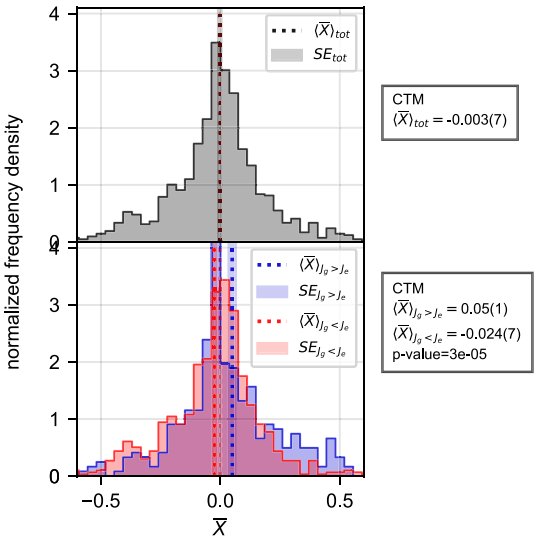

Fig. 4 Top: $\overline{X}$ distribution for the complete set of data using CTM and $R_{sc} = 1.0$. Bottom: $\overline{X}$ distributions dividing the dataset based on the difference between spins of produced nucleus ground and excited states. All three histograms are normalized with respect to the number of entries contained as well as step size

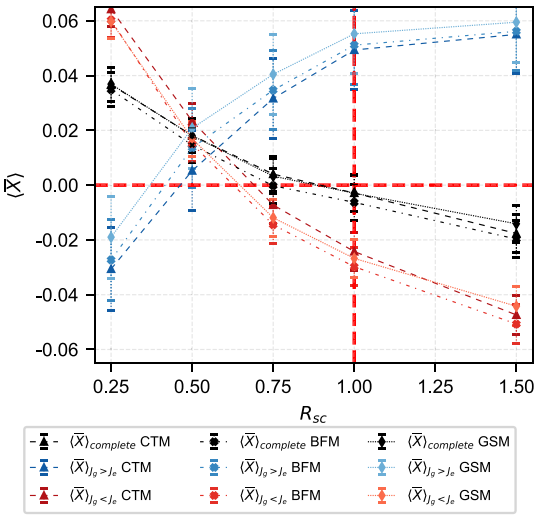

Fig. 5 Trend of $\langle\overline{X}\rangle$ as a function of R_{sc} for empirical LDMs

Possible systematic effects can be studied by repeating the same process on limited parts of the dataset, decomposing it into groups of entries sharing common features. The bottom plot in Fig. 4 shows the distributions collecting nuclei based on whether the ground state spin J_g is smaller (803 entries) or larger (328 entries) than that of the excited state J_e. The two histograms display opposite trends, and indeed this difference is also confirmed by the respective average values of $\overline{X}$, as $\langle\overline{X}\rangle_{J_g<J_e} = -0.027(7)$ while $\langle\overline{X}\rangle_{J_g>J_e} = 0.04(1)$. Moreover, the two-sample Kolmogorov-Smirnov test applied to the two distributions returns a very small p-value of $5 \cdot 10^{-5}$, far below the conventional significance level of 0.05. This means that the two distributions are significantly different. Table 2 shows the result of this comparison for all six LDMs implemented in TALYS, i.e., even the three microscopic LDMs not included in further steps of this work. As can be seen, the observed behaviour is similar for all the six LDMs. On average, the three phenomenological models perform slightly better and the observed preference of populating the high spin state is somewhat more pronounced in the case of the three microscopic models.

To investigate the dependence of this bias with respect to the width of the spin distribution, as already introduced, the calculations and analysis process have then been repeated varying the multiplying factor R_{sc} and studying the impact on $\langle\overline{X}\rangle$, $\langle\overline{X}\rangle_{J_g<J_e}$, and $\langle\overline{X}\rangle_{J_g>J_e}$.

6 Results and discussion

The behaviour observed using the default settings of TALYS (Fig. 4) shows that the code performs differently depending on the spin of the two nuclear states; specifically, the models implemented in TALYS tend to overestimate the yield of high-spin states with respect to the low-spin ones. When the ground state is the high spin state, one can observe that $\langle\overline{X}\rangle > 0$, thus on average for these entries $\mathrm{IYR_{exp}}$ is larger than $\mathrm{IYR_{TALYS}}$. When on the other hand the excited state is the high spin state, we derive that $\langle\overline{X}\rangle < 0$ and it follows that on average $\mathrm{IYR_{TALYS}} > \mathrm{IYR_{exp}}$.

Figure 5 shows how the $\langle\overline{X}\rangle$ evolves with respect to R_{sc} for the three phenomenological LDMs. The calculations show a similar trend for all the LDMs, with the convergence of the $\langle\overline{X}\rangle$ values for $R_{sc} \approx 0.5$. Additionally, Fig. 6 displays the p-value of the Kolmogorov-Smirnov test calculated for all these distributions, which is relevant in this case because the greater the p-value, the higher the probability that the two distributions are equivalent. From this plot, it may be inferred

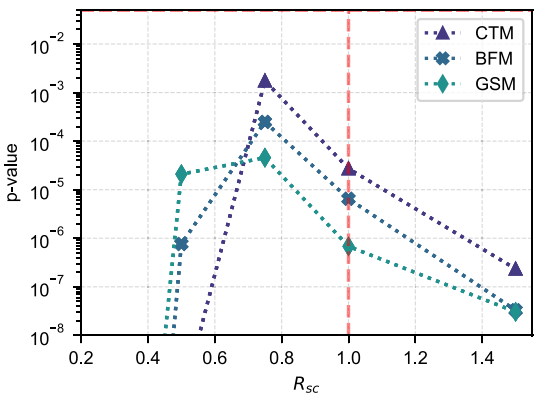

Fig. 6 P-value of Kolmogorov-Smirnov test applied to the $\overline{X}$ distributions for $J_g \lessgtr J_e$ sub-sets as a function of R_{sc} for the three phenomenological LDMs. Values below 10^{-8} are not shown

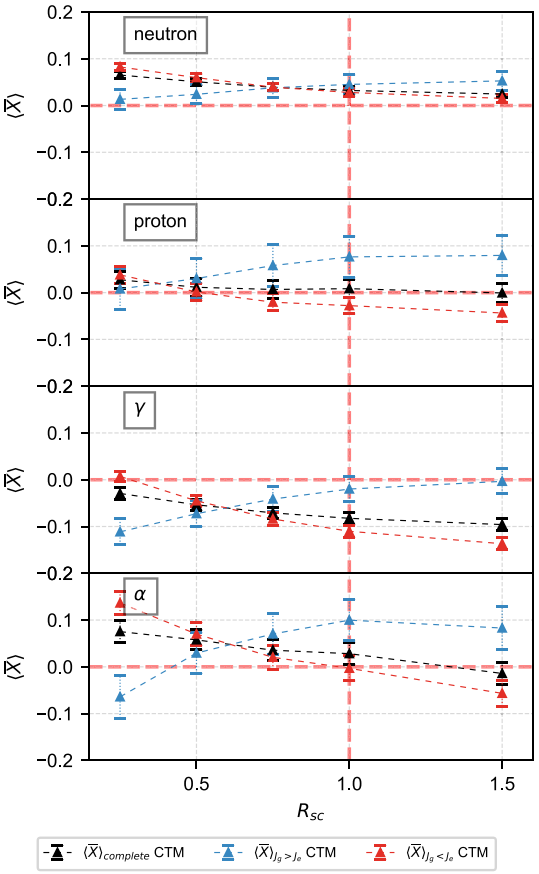

Fig. 7 Trends of $\langle X\rangle$ as a function of R_{sc} for the subsets corresponding to reactions involving different projectiles using CTM as LDM

that using $R_{sc} \approx 0.75$ the distributions become more similar, although not equivalent considering that the p-value is still far below the threshold significance level of 0.05.

It is also possible to divide the full dataset of reactions into sub-sets depending on the projectile particle involved, to study if the showed behaviour can be related to one specific particle. The results are shown in Fig. 7. While all projectiles display similar trends with respect to the change in R_{sc}, several differences can be observed. Data from neutron-induced reactions show the least spread between $\langle X\rangle_{J_g \lessgtr J_e}$ and an optimal value closer to $R_{sc} \approx 0.75$. The reactions induced by protons, α-particles and γ-rays seem to need even smaller values of Rsc, showing best results for values around $R_{sc} \approx 0.5$. These differences might be due a different performance on the description of the entrance channel.

Nonetheless, even though different sub-sets show different biases on $\langle X\rangle_{J_g \lessgtr J_e}$, and suggesting one specific global value for R_{sc} seems not possible, it is clear that a significant reduction of R_{sc} improves the agreement between calculated and measured IYR values.

This implies that a reduction of the width of the LD's spin distribution is needed in order to improve, on average, the performances of the phenomenological models used by TALYS. Qualitatively, such a decrease translates into a lower mean value for the Rayleigh distribution (in Eq. 3), hence a higher occupancy of low spin states, while suppressing transitions to higher spin states. This conclusion is also supported by the recent work of Hilaire et al. [29]. Using a new approach, i.e., the boson expansion of QRPA excitations, they calculate nuclear level densities that present a rather narrow spin distribution and achieve promising results.

There are several possible explanations for this result. One might be that the assumption of random coupling of the angular momentum projections entering the derivation of Eq. 4 [30,31] is not generally valid, and that a more quenched distribution than the used Rayleigh distribution is needed to describe spin populations in the LDM. Another, maybe more likely possibility is that the spin cut-off parameter is generally overestimated in the modeling. The reason might be that the moments-of-inertia used to describe collective rotational excitations are overestimated as suggested by, e.g., Sudár and Qaim [18].

7 Summary and outlook

We have performed a comparison of calculated versus experimentally obtained IYR for spin isomers across the nuclear chart. An extensive set of calculations was performed with TALYS 1.96, invoking three phenomenological and three microscopic LDM, for a total of 1130 EXFOR entries with 5359 experimental data points. We observed significant favouring of the population of high spin states for default model calculations ($R_{sc} = 1.0$).

For the three phenomenological LDMs, calculations were then repeated for 5 different R_{sc} values, ranging from 0.25 to 1.5. We found that a value of R_{sc} smaller than the default one is needed to mitigate this behaviour and achieve better agreement between model calculations and experimental observations. Our findings are in line with what was found in previous works which looked at specific reactions or a subset of IYRs [16,18–20]. Implementing an improved parametrisation to calculate the spin cut-off parameter in a later version of TALYS would improve its predictive power for isomeric production and possibly for gamma-ray production cross sections.

The experimental data in this study cover nuclei over a wide range of masses in the nuclear chart, several projectile particles, and energies. We, therefore, acknowledge that the suggested R_{sc} value may vary considerably regarding what is optimal for any specific nuclei. It would be useful to extend this study and in particular investigate the impact of initial excitation energy and nuclear deformation.

As examples, we mention two important consequences. The first concerns the angular momentum of fission frag-

ments derived from measured IYR. The reduced width of the spin distribution suggested by our work may imply that the angular momentum of fission fragments calculated on the basis of observed IYRs in previous works [10–12] needs to shift to larger average values, provided that this result is confirmed also for microscopic LDMs. This would then also have an impact on neutron and gamma-ray multiplicities as observed by Piau et al. [20]. Another consequence is that a smaller width of the spin distributions in the current modelling of fission fragment de-excitation leads to different de-excitation paths and different IYR for the fission products, and changes the feeding of the states undergoing beta-decay. This variation could have an impact on the fission observables based on the yield after the decay process, such as the calculated antineutrino energy spectra emitted, e.g., from nuclear reactor cores, as they depend on fission yields [32].

Acknowledgements This work was supported by the Swedish Research Council (Ref. No. 2020-04238).

Funding Open access funding provided by Uppsala University.

Data Availability Statement This manuscript has no associated data or the data will not be deposited. [Authors' comment: The datasets generated and/or analyzed during the current study are publicly available and repro- ducible in/by the open-source nuclear reaction model code, TALYS.]

References

1. J.B. Wilhelmy, E. Cheifetz, R.C. Jared, S.G. Thompson, H.R. Bowman, J.O. Rasmussen, Angular Momentum of Primary Products Formed in the Spontaneous Fission of Cf 252. Phys. Rev. C **5**(6), 2041–2060 (1972). https://doi.org/10.1103/PhysRevC.5.2041
2. A.N. Andreyev, K. Nishio, K.-H. Schmidt, Nuclear fission: A review of experimental advances and phenomenology. Rep. Prog. Phys. **81**(1), 016301 (2018). https://doi.org/10.1088/1361-6633/aa82eb
3. J.N. Wilson, D. Thisse, M. Lebois, N. Jovančević, D. Gjestvang, R. Canavan, M. Rudigier, D. Étasse, R.-B. Gerst, L. Gaudefroy, E. Adamska, P. Adsley, A. Algora, M. Babo, K. Belvedere, J. Benito, G. Benzoni, A. Blazhev, A. Boso, S. Bottoni, M. Bunce, R. Chakma, N. Cieplicka-Oryńczak, S. Courtin, M.L. Cortés, P. Davies, C. Delafosse, M. Fallot, B. Fornal, L. Fraile, A. Gottardo, V. Guadilla, G. Häfner, K. Hauschild, M. Heine, C. Henrich, I. Homm, F. Ibrahim, ŁW. Iskra, P. Ivanov, S. Jazrawi, A. Korgul, P. Koseoglou, T. Kröll, T. Kurtukian-Nieto, L. Le Meur, S. Leoni, J. Ljungvall, A. Lopez-Martens, R. Lozeva, I. Matea, K. Miernik, J. Nemer, S. Oberstedt, W. Paulsen, M. Piersa, Y. Popovitch, C. Porzio, L. Qi, D. Ralet, P.H. Regan, K. Rezynkina, V. Sánchez-Tembleque, S. Siem, C. Schmitt, P.-A. Söderström, C. Sürder, G. Tocabens, V. Vedia, D. Verney, N. Warr, B. Wasilewska, J. Wiederhold, M. Yavahchova, F. Zeiser, S. Ziliani, Angular momentum generation in nuclear fission. Nature **590**(7847), 566–570 (2021). https://doi.org/10.1038/s41586-021-03304-w
4. J. Randrup, R. Vogt, Generation of Fragment Angular Momentum in Fission. Phys. Rev. Lett. **127**(6), 062502 (2021). https://doi.org/10.1103/PhysRevLett.127.062502
5. A. Bulgac, The angular correlation between the fission fragment intrinsic spins. Phys. Rev. C **106**(1), 014624 (2022). https://doi.org/10.1103/PhysRevC.106.014624. arXiv:2108.07268 [nucl-ex, physics:nucl-th, physics:quant-ph]
6. R. Vogt, J. Randrup, Angular momentum effects in fission. Phys. Rev. C **103**(1), 014610 (2021). https://doi.org/10.1103/PhysRevC.103.014610
7. P. Marević, N. Schunck, J. Randrup, R. Vogt, Angular momentum of fission fragments from microscopic theory. Phys. Rev. C **104**(2), 021601 (2021). https://doi.org/10.1103/PhysRevC.104.L021601
8. J.R. Huizenga, R. Vandenbosch, Interpretation of Isomeric Cross-Section Ratios for (n, γ) and (γ, n) Reactions. Phys. Rev. **120**(4), 1305–1312 (1960). https://doi.org/10.1103/PhysRev.120.1305
9. R. Vandenbosch, J.R. Huizenga, Isomeric Cross-Section Ratios for Reactions Producing the Isomeric Pair Hg 1 9 7, 1 9 7 m. Phys. Rev. **120**(4), 1313–1318 (1960). https://doi.org/10.1103/PhysRev.120.1313
10. V. Rakopoulos, M. Lantz, A. Solders, A. Al-Adili, A. Mattera, L. Canete, T. Eronen, D. Gorelov, A. Jokinen, A. Kankainen, V.S. Kolhinen, I.D. Moore, D.A. Nesterenko, H. Penttilä, I. Pohjalainen, S. Rinta-Antila, V. Simutkin, M. Vilén, A. Voss, S. Pomp, First isomeric yield ratio measurements by direct ion counting and implications for the angular momentum of the primary fission fragments. Phys. Rev. C **98**(2), 024612 (2018). https://doi.org/10.1103/PhysRevC.98.024612
11. V. Rakopoulos, M. Lantz, S. Pomp, A. Solders, A. Al-Adili, L. Canete, T. Eronen, A. Jokinen, A. Kankainen, A. Mattera, I.D. Moore, D.A. Nesterenko, M. Reponen, S. Rinta-Antila, A. De Roubin, M. Vilén, M. Österlund, H. Penttilä, Isomeric fission yield ratios for odd-mass cd and in isotopes using the phase-imaging ion-cyclotron-resonance technique. Phys. Rev. C (2019). https://doi.org/10.1103/PhysRevC.99.014617
12. A. Al-Adili, V. Rakopoulos, A. Solders, Extraction of angular momenta from isomeric yield ratios: employing talys to de-excite primary fission fragments. Eur. Phys. J. A (2019). https://doi.org/10.1140/epja/i2019-12731-5
13. A.J. Koning, D. Rochman, Modern nuclear data evaluation with the TALYS code system. Nucl. Data Sheets **113**(12), 2841–2934 (2012). https://doi.org/10.1016/j.nds.2012.11.002
14. A. Koning, S. Hilaire, S. Goriely, Talys: modeling of nuclear reactions. Eur. Phys. J. A (2023). https://doi.org/10.1140/epja/s10050-023-01034-3
15. EXFOR: Experimental Nuclear Reaction Data. https://www-nds.iaea.org/exfor/
16. A. Rodrigo, N. Otuka, S. Takács, A.J. Koning, Compilation of isomeric ratios of light particle induced nuclear reactions. Atomic Data Nucl. Data Tables (2023). https://doi.org/10.1016/j.adt.2023.101583
17. C.J. Sears, A. Mattera, E.A. McCutchan, A.A. Sonzogni, D.A. Brown, D. Potemkin, Compilation and evaluation of isomeric fission yield ratios. Nucl. Data Sheets **173**, 118–143 (2021). https://doi.org/10.1016/j.nds.2021.04.005
18. S. Sudár, S.M. Qaim, Mass number and excitation energy dependence of the $\theta_{eff}/\theta_{rig}$ parameter of the spin cut-off factor in the

formation of an isomeric pair. Nucl. Phys. A **979**, 113–142 (2018). https://doi.org/10.1016/j.nuclphysa.2018.09.039
19. M. Uddin Khandaker, A. Kumer Chakraborty, K. Nagatsu, K. Minegishi, M.-r Zhang, Measurement and calculation of isomeric cross section ratios for the natw(3he, x)184m, gre reactions. Nucl. Instrum. Methods Phys. Res. Sect. B **536**, 11–17 (2023). https://doi.org/10.1016/j.nimb.2022.12.018
20. V. Piau, O. Litaize, A. Chebboubi, S. Oberstedt, A. Göök, A. Oberstedt, Neutron and gamma multiplicities calculated in the consistent framework of the hauser-feshbach monte carlo code fifrelin. Phys. Lett. Sect. B Nucl. Elementary Particle High-Energy Phys. **10**, 10 (2023). https://doi.org/10.1016/j.physletb.2022.137648
21. A. Gilbert, A.G.W. Cameron, A composite nuclear-level density formula with shell corrections. Can. J. Phys. **43**(8), 1446–1496 (1965). https://doi.org/10.1139/p65-139
22. W. Dilg, W. Schantl, H. Vonach, M. Uhl, Level density parameters for the back-shifted fermi gas model in the mass range 40 < a < 250. Nucl. Phys. A **217**(2), 269–298 (1973). https://doi.org/10.1016/0375-9474(73)90196-6
23. A.V. Ignatyuk, K.K. Istekov, G.N. Smirenkin, Role of collective effects in the systematics of nuclear level densities. Sov. J. Nucl. Phys. (Engl. Transl.); (United States) **29**(4), (1979)
24. P. Demetriou, S. Goriely, Microscopic nuclear level densities for practical applications. Nucl. Phys. A **695**(1), 95–108 (2001). https://doi.org/10.1016/S0375-9474(01)01095-8
25. S. Goriely, S. Hilaire, A.J. Koning, Improved microscopic nuclear level densities within the hartree-fock-bogoliubov plus combinatorial method. Phys. Rev. C **78**, 064307 (2008). https://doi.org/10.1103/PhysRevC.78.064307
26. S. Hilaire, M. Girod, S. Goriely, A.J. Koning, Temperature-dependent combinatorial level densities with the d1m gogny force. Phys. Rev. C **86**, 064317 (2012). https://doi.org/10.1103/PhysRevC.86.064317
27. A.J. Koning, S. Hilaire, S. Goriely, Global and local level density models. Nucl. Phys. A **810**(1–4), 13–76 (2008). https://doi.org/10.1016/j.nuclphysa.2008.06.005
28. H. Vignau, S.J. Nassiff, Yield Ratios of the Isomeric Pair $Ce^{137}m/^{137}$ Formed by La^{139}(d, 4n)Ce^{137} Reaction. Nucl. Phys. **26**, 108 (1961). https://doi.org/10.1016/0029-5582(61)90120-1
29. S. Hilaire, S. Goriely, S. Péru, G. Gosselin, A new approach to nuclear level densities: the qrpa plus boson expansion. Phys. Lett. B **843**, 137989 (2023). https://doi.org/10.1016/j.physletb.2023.137989
30. H.A. Bethe, Nuclear physics b. nuclear dynamics, theoretical. Rev. Mod. Phys. **9**, 69–244 (1937). https://doi.org/10.1103/RevModPhys.9.69
31. T. Ericson, The statistical model and nuclear level densities. Adv. Phys. **9**(36), 425–511 (1960). https://doi.org/10.1080/00018736000101239
32. A.A. Sonzogni, E.A. McCutchan, T.D. Johnson, P. Dimitriou, Effects of fission yield data in the calculation of antineutrino spectra for ^{235}U(n, fission) at thermal and fast neutron energies. Phys. Rev. Lett. **116**, 132502 (2016). https://doi.org/10.1103/PhysRevLett.116.132502